(Received 27 September 2023, Accepted 12 January 2024, Scheduled 26 January 2024)

4-Ports Small Size Metamaterial Antenna with Electromagnetic Walls for MIMO Systems

Cristopher Pineda-Salgado[1], José A. Tirado-Méndez[1,*], Hildeberto Jardon-Aguilar[2], Ruben Flores-Leal[2], Arturo Rangel-Merino[1], and Jaime P. Abarca-Reyna[1]

[1]*National Polytechnic Institute, ESIME Zacatenco, Av. IPN S/N, Edif. 5, CDMX 07300, Mexico*
[2]*CINVESTAV-IPN, Telecommunications Section, Av. IPN 2508, CDMX 07360, Mexico*

ABSTRACT: In this paper, a very small 4-port MIMO antenna is designed, based on a metamaterial structure composed of embedded octagonal Split-Ring Resonators (SSRs). The antenna array shows an axial symmetry configuration with dimensions of $32 \times 32\,\text{mm}^2$, corresponding to $0.157\lambda^2$, approximately, related to a center frequency of 3.5 GHz, with a high electromagnetic isolation despite the radiators' closeness, reaching values bigger than 26 dB for adjacent antennas, and more than 28 dB for opposite antennas. The antenna is built on a substrate with dielectric permittivity of 2.2 and 1.27 mm thick. The Total Active Reflection Coefficient (*TARC*) presents a steady behavior for different random phases at the incoming signals, keeping a system bandwidth of 0.9 GHz for a -10 dB value. On the other hand, the Envelope Correlations Coefficient (*ECC*) reports values lower than 0.001 in all the antenna relationships, achieving a very uncorrelated performance of the electric fields in each element. The radiation pattern is quasi-omnidirectional, obtaining a low gain around -2 dBi, a trade-off that is considering the size reduction of the MIMO antenna.

1. INTRODUCTION

Current mobile communications require high data rates to satisfy the users' necessities. To increase these rates, various strategies can be employed, and one of them is the use of Multiple Input-Multiple Output (MIMO) antenna arrays, in order to take advantage of multipath effects, especially in mobile environments. Due to these factors, the antennas in mobile systems require very restrictive characteristics that allow them to operate in such adverse environments, without causing distortions in the desired signals. Because the mobile is a system that has space limitations, small antennas are mandatory, but at the same time, they must have an ideal performance in hostile multipath conditions. The low correlation between the electric fields of each element that makes up the MIMO array, the high electromagnetic isolation among radiators, as well as a stable behavior of the bandwidth when there are different signals in each antenna of the array, and high diversity gain, are some of the characteristics that have to be satisfied, among other factors. All these characteristics are naturally opposed to the reduction in the size of the antenna, due to the proximity of the elements, resulting in an increase in their interaction, reducing electromagnetic isolation, and growing the correlation between fields.

To achieve the different goals of a MIMO array, different proposals have been made to reduce the size, by using geometries [1] and element interconnections [2]. On the other hand, to increase the electromagnetic isolation, several proposals have been published, including slots and shorting pins [3], Defected Ground Structures [4, 5], electromagnetic barriers, and imperfect structures, among other techniques.

In this work, a metamaterial structure is used to increase the electrical length of the radiator, in such a way that an antenna with reduced dimensions is obtained in comparison with a conventional antenna, such as a circular monopole.

Metamaterial is a media in which its physical characteristics and the propagating wave on it are determined by negative dielectric and magnetic constitutive parameters. In such media, the electromagnetic fields and the wavevector form a left-handed triad. This means that the group and phase velocity have opposite directions. This phenomenon can be employed to enhance the electrical characteristics of passive circuits, in this case antennas. Reducing the size of radiators by employing reactive loads or shorting pins can result in poor radiation, narrow bandwidth, and non-desired radiation. The use of metamaterial has been proven to be an option to improve some electric characteristics of antennas, such as those demonstrated in [6–8]. In those works, efficient antennas were developed for applications like WiMAX, WiFi, wireless, and personal applications, respectively, showing the potential of employing this kind of technique.

To improve the isolation without increasing size or volume, simple electromagnetic barriers are introduced, which are easy to implement and design, based on tape-type transmission lines. The proposed structure and its simulation and measurement results are shown in the following sections.

2. MIMO ANTENNA PROPOSAL

The proposed configuration of the metamaterial antenna is presented in Figure 1(b), taking into account that the SRR has been proven to perform as a metamaterial structure in several publications [9, 10]. To initiate the design and for comparison pur-

* Corresponding author: José Alfredo Tirado-Méndez (jtiradom@ipn.mx).

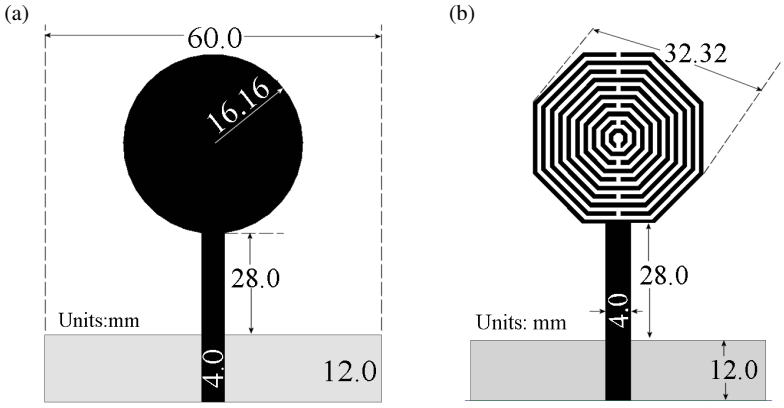

FIGURE 1. Comparison of: (a) conventional disc monopole, (b) metamaterial based monopole.

poses, Equations (1) and (2) in [11] are considered for a disc monopole design, resonating at 3.5 GHz. According to these equations, the radius of the disc monopole is around 16.16 mm. The disc monopole is displayed in Figure 1(a). Both antennas are simulated considering a substrate with dielectric permittivity of 2.2 and thickness of 1.27 mm. As a monopole structure, the resonance of the antenna is determined by the length of the feeding line starting from the edge of the ground plane and complemented by the reactive load generated by the disc. The same phenomenon is used for the metamaterial-based antenna; however, the reactive load is bigger in the second option, as will be shown below. In the case of the metamaterial-based antenna, it is excited by a microstrip line and terminated in the embedded SRRs. These rings act as the radiation part of the antenna but add a load to the transmission line. As explained above, metamaterial allows to obtain a phase velocity contrary to the propagation direction, which increases the slow-wave factor in the structure. This fact permits obtaining a shorter wavelength, and as a result, the physical size of the antenna can also be reduced.

As observed in Figure 1, the two antennas have the same dimensions. The metamaterial-based antenna shows 10 SRRs, and each one is 0.8 mm in width and separated also by 0.8 mm. The simulated S_{11} parameters for each antenna are given in Figure 2.

In Figure 2, the S_{11} parameter for the disc monopole antenna presents a resonance around 3.5 GHz, which is the design frequency; however, when the metamaterial configuration is used, the resonance of the structure is obtained at a lower frequency, around 1.8 GHz. According to these results, the employment of SRRs in the structure increases the slow-wave factor, reducing the electric length of the radiator, and as a consequence, a lower resonance is obtained. To shift the resonance of the metamaterial-based antenna to 3.5 GHz, its dimensions must be reduced. This process was made and optimized by employing the Optimetrics Tool of the electromagnetic simulator HFSS. The final dimensions of the metamaterial-based antenna are presented in Figure 3, as well as its simulated S_{11} parameter.

From Figure 3, it is observed that the dimensions of the metamaterial-based antenna were reduced almost four times compared to the dimensions presented in Figure 1(b), and the

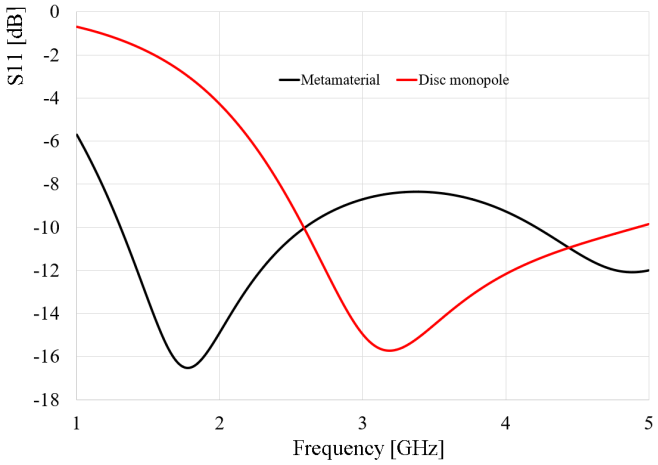

FIGURE 2. Simulated S_{11} parameter of the metamaterial-based and disc monopole antennas.

resonance of the antenna is obtained at 3.5 GHz. Then, the size of the metamaterial-based antenna is reduced to an equivalent of around 25% of the total dimension of the conventional disc monopole. This size reduction is given by the metamaterial effect of the SRRs. To demonstrate this behavior, the extraction of the permittivity of the structure is given below.

To obtain the permittivity, the antenna is arranged as pictured in Figure 4. The feeding port is set at the feeding line, and the receiving port is set above the antenna, on the upper face of the radiation boundary.

According to Equations (1) to (4) [12], the extracted permittivity based on the S-parameters is obtained and plotted in Figure 5.

$$z = \pm\sqrt{\frac{(1+S_{11})^2 - S_{21}^2}{(1-S_{11})^2 - S_{21}^2}} \tag{1}$$

$$n = \pm\frac{1}{jL}\left(\frac{c}{\omega}\right)\cosh^{-1}\left(\frac{1-S_{11}^2+S_{21}^2}{2S_{21}}\right) \tag{2}$$

The signs in (1) and (2) are determined by:

$$z' \geq 0 \tag{3}$$

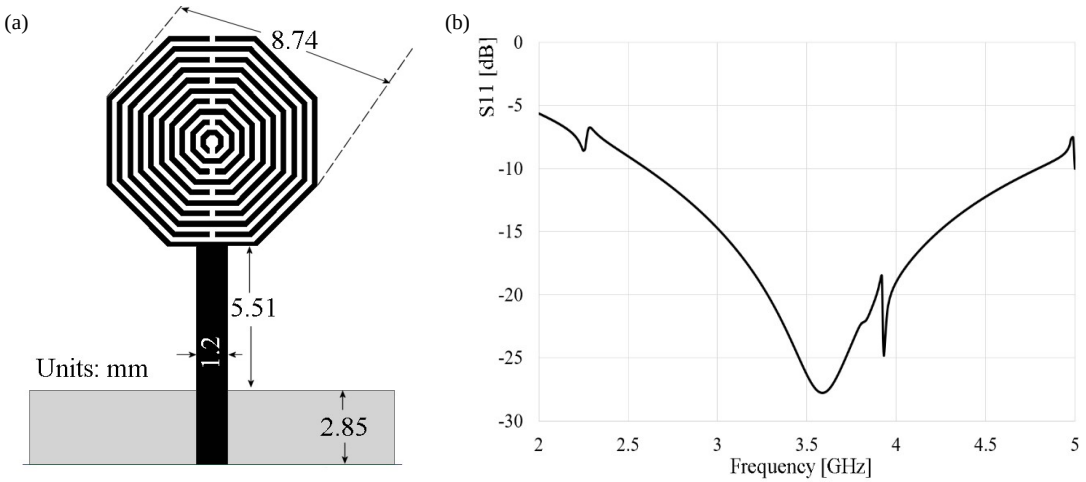

FIGURE 3. (a) Metamaterial-based optimized antenna and (b) simulated S_{11} parameter.

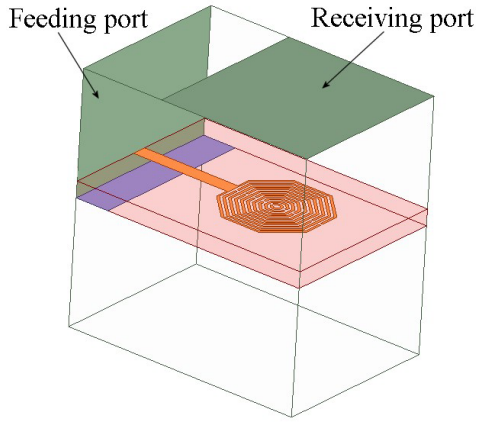

FIGURE 4. Simulation model to extract the permittivity of the metamaterial-based structure.

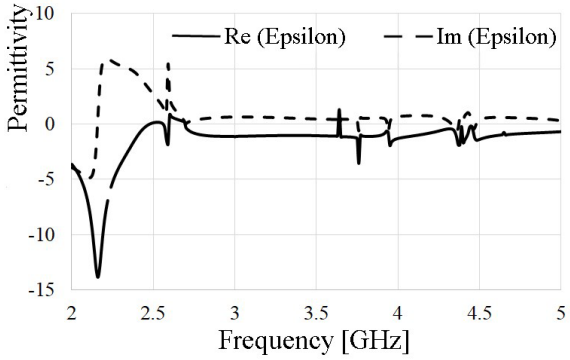

FIGURE 5. Extracted permittivity of the metamaterial-based antenna.

$$n'' \geq 0 \tag{4}$$

where $\mu = nz$ and $\varepsilon = n/z$, with n being the refractive index.

As observed in Figure 5, the extracted permittivity of the metamaterial-based antenna presents a real part negative value at the resonant frequency, demonstrating the metamaterial performance at the desired band. As a result, the slow wave factor on the structure is bigger than that shown on a conventional disc monopole, giving a resonance of around 3.5 GHz, with a much smaller size radiator.

According to previous results, the reduction of the antenna compared to a conventional disc radiator is close to 75%. Then, the following section demonstrates the performance of a 4-port MIMO array, considering the antenna presented in Figure 3.

3. 4-PORT MIMO ANTENNA ARRAY

The proposed 4-port antenna array is presented in Figure 6. The dimension variables of the antenna are presented in the same figure and are as follows: $Wg = 2.85\,\text{mm}$, $Lg = 14\,\text{mm}$, $Wf = 1.213\,\text{mm}$, $Lf = 8.36\,\text{mm}$, $R = 8.03\,\text{mm}$, $Lr = 3.34\,\text{mm}$, $La = 34\,\text{mm}$, $Ld = 18.3\,\text{mm}$, $As = 5.06\,\text{mm}$, $Gs = 4.59\,\text{mm}$, the electromagnetic walls are 0.75 mm wide

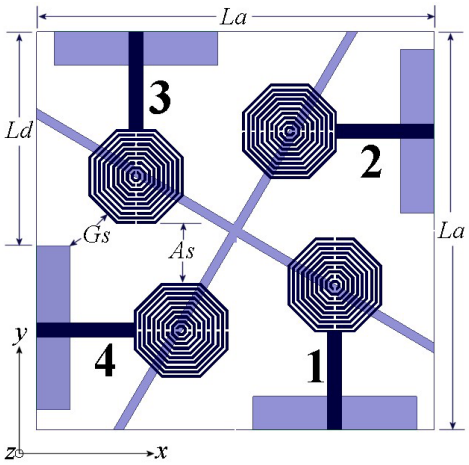

FIGURE 6. Proposed metamaterial antenna array configuration and dimensions.

and 39.4 mm long. Each octagonal ring width as well as the separation among them is set to 0.2 mm. These dimensions were obtained after an optimization process using HFSS, achieving the best port matching and bandwidth considering an $S_{11} \leq -10\,\text{dB}$. The antenna array is simulated considering a substrate

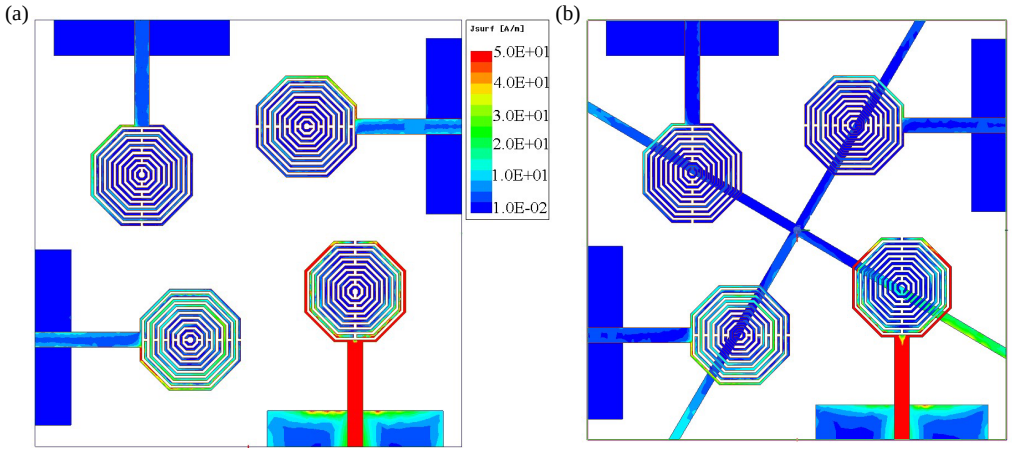

FIGURE 7. Comparison of current distribution, (a) without EM walls, (b) with EM walls.

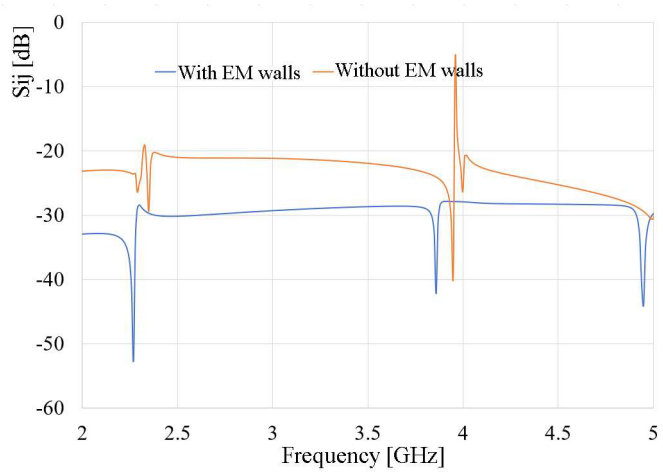

FIGURE 8. Comparison of simulated isolation with and without EM walls.

with dielectric permittivity of 2.2 and thickness of 1.27 mm. The SRR has been probed to perform as a metamaterial structure, then, its behavior is exploited to increase the electric length of the structure; in this way, the antenna resonates at the desired frequency using a small dimension compared to a conventional monopole.

The 4-element array presents an axial symmetry, in which the radiators are placed orthogonally to each other. With this arrangement, the electric fields are also orthogonally arranged, and as a result, the correlation among fields is reduced. Also, each radiator has its ground plane, avoiding the induced field on this side of the substrate due to the surface mode propagation fields. This fact is corroborated when the Envelope Correlation Coefficient (*ECC*) is calculated. Since all non-ideal radiators present cross-polarization, and due to the closeness among antennas in the array, some electric coupling can arise. To increase the electromagnetic (EM) isolation among elements, EM walls were introduced on the ground plane. These structures are very simple to design and implement, but they are highly effective in isolating electromagnetically. The width of these lines was obtained by a simulation process, achieving a value of 0.75 mm. The intersection of the EM walls is located at the center of the array and extended to the edges of the substrate, passing just below the center of each SRR set. The current distribution analysis is made using HFSS, and the results are presented in Figure 7, where the structure is analyzed with and without EM walls. As a result, it is observed that the intensity of the surface current distribution induced by the surrounding radiators is reduced considerably when the EM walls are used. These lines do not modify, considerably, the frequency response of the radiators as well as the radiation pattern, but increase the EM isolation by more than 6 dB at 3.5 GHz, compared to when the structures are not employed. The isolation among radiators is given by the Sij parameter, and the results are presented in Figure 8.

4. SIMULATED AND MEASURED RESULTS

The prototype of the 4-port MIMO antenna is presented in Figure 9. Figure 9(a) displays the front layer, where the radiators are placed, and Figure 9(b) shows the back view, where the electromagnetic walls and ground planes are located.

The array was characterized, and a comparison of the simulated and measured results of the S-parameters is given in Figure 10. Due to the symmetry of the configuration, for clearance in the graphics, just the parameters related to port 1 are pre-

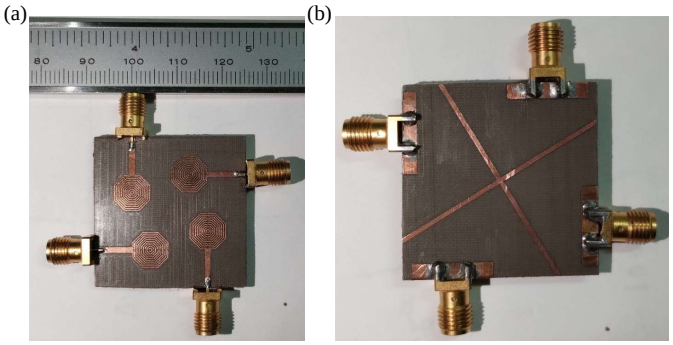

FIGURE 9. 4-ports MIMO antenna prototype.

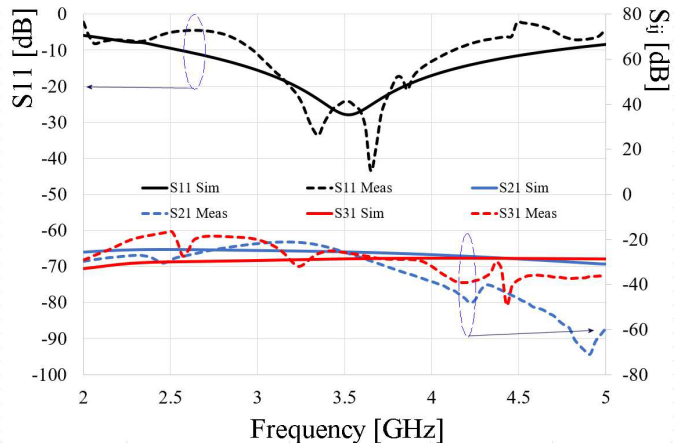

FIGURE 10. Comparison of simulated and measured S-parameters of the MIMO antenna.

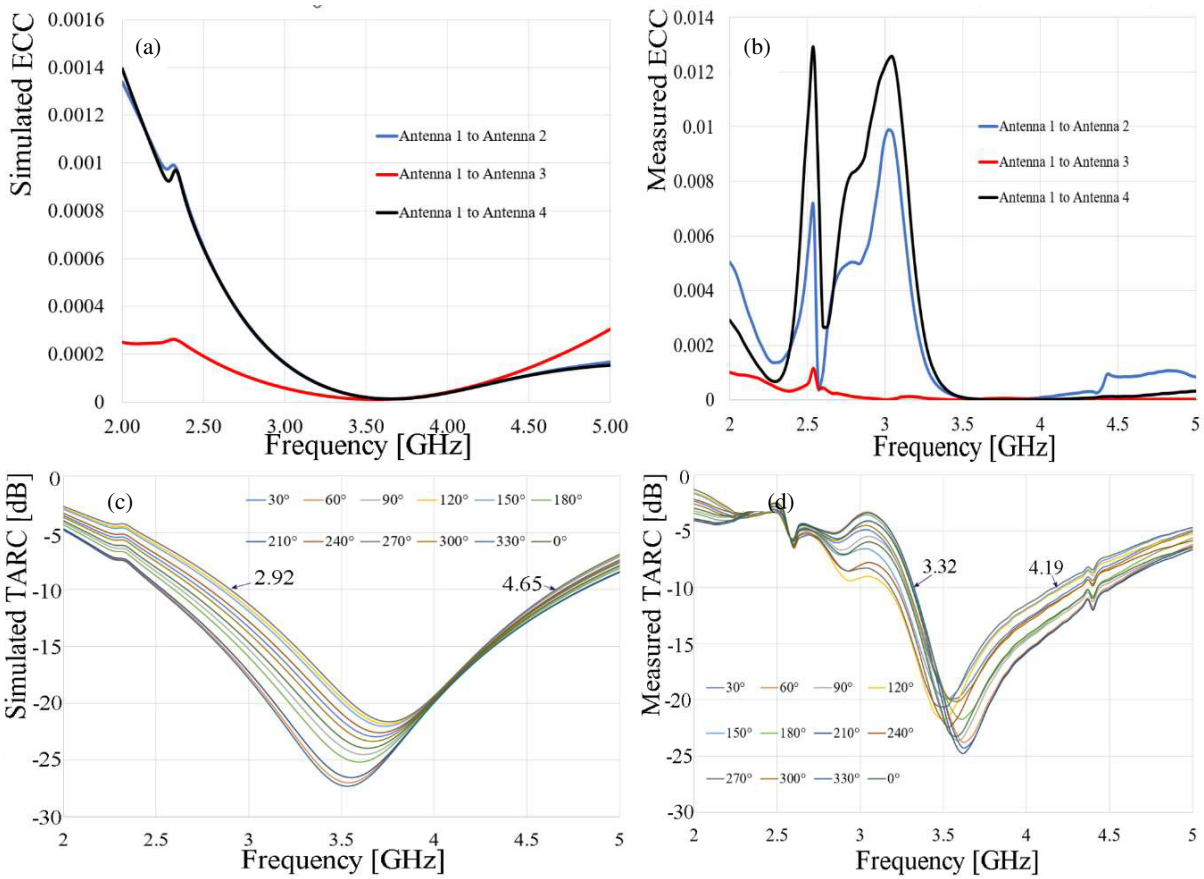

FIGURE 11. Simulated and measured ECC and TARC of the MIMO antenna, (a) simulated ECC, (b) measured ECC, (c) simulated TARC, (d) measured TARC.

sented, since $S_{11} = S_{22} = S_{33} = S_{44}$, and $S_{ij} = S_{ji}$, where i and j go from 1 to 4.

From Figure 10, it is observed that the simulated and measured parameters show great convergence, obtaining a measured bandwidth from 2.99 to 4.13 GHz, while the isolation among radiators described by the S_{ij} parameters reaches values of more than 25 dB for adjacent and opposite antennas.

On the other hand, the MIMO metrics like *ECC*, *DG* [13, 15], and *TARC* [14] are described by (5), (6), and (7), respectively, where N is the number of elements in the array.

$$ECC = \frac{\left|S_{11}^{*}S_{12} + S_{21}^{*}S_{22}\right|^{2}}{\left(1 - \left|S_{11}\right|^{2} - \left|S_{21}\right|^{2}\right)\left(1 - \left|S_{22}\right|^{2} - \left|S_{12}\right|^{2}\right)} \quad (5)$$

$$DG = 10\sqrt{1 - (ECC)^{2}} \quad (6)$$

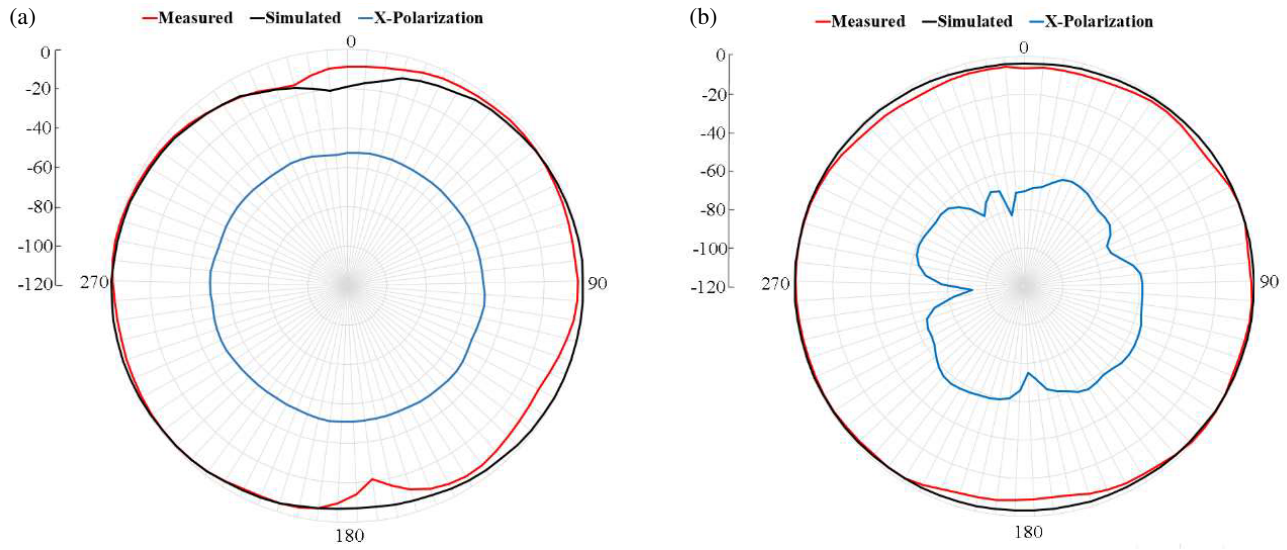

FIGURE 12. Normalized gain pattern in dBi at 3.5 GHz, (a) E-plane, (b) H-plane.

TABLE 1. Comparison of 4-elements MIMO antennas with the present work.

Reference	ECC	DG	TARC [dB]	Operating Frequency [GHz]	Size (λ_0^2) [mm^2]	Fractional BW [%]
[2]	≤ 0.001	10	$\leq -10*$	3.5	1.53	5.7
[3]	≤ 0.001	10	NA	3.5	3.062	15.7
[4]	≤ 0.001	10	≤ -10	28	6.97	10.7
[19]	10E-4	10	$\leq -10*$	13.5	4.86	1.5
[20]	≤ 0.001	9.99	NA	5.9	2.11	7.6
[21]	≤ 0.004	NA	NA	3	0.5	26.6
This work	$\leq$ 8E-5	10	≤ -10	3.5	0.157	34.2

$$TARC = N^{-0.5}\sqrt{\sum_{i=1}^{N}\left|\sum_{k=1}^{N} S_{ik}e^{j\theta_{k-1}}\right|^2} \quad (7)$$

The corresponding values of the simulated and measured results of these metrics are displayed in Figure 11.

In Figure 11, the simulated *ECC* reaches values as low as 0.0001 at the desired frequency, while the measured one gets values lower than 0.001, showing a great result since very poorly correlated electric fields among radiators are obtained. According to (6), the Diversity Gain (*DG*), at the resonant frequency, gives a value close to 10 either for simulation or measured results.

On the other hand, following Equation (7), for a four-element array, the *TARC* can be expanded to (8).

$$\begin{aligned} TARC = 4^{-0.5}\Big[&\left|S_{11}+S_{12}e^{j\theta_1}+S_{13}e^{j\theta_2}+S_{14}e^{j\theta_3}\right|^2 \\ &+\left|S_{21}+S_{22}e^{j\theta_1}+S_{23}e^{j\theta_2}+S_{24}e^{j\theta_3}\right|^2 \\ &+\left|S_{31}+S_{32}e^{j\theta_1}+S_{33}e^{j\theta_2}+S_{34}e^{j\theta_3}\right|^2 \\ &+\left|S_{41}+S_{42}e^{j\theta_1}+S_{43}e^{j\theta_2}+S_{44}e^{j\theta_3}\right|^2\Big]^{0.5} \end{aligned} \quad (8)$$

According to (8), the *TARC* is dependent on three different phases that can be random, giving as a result a set of curves as big as the number of phases selected for the analysis. To simplify the outcome, a small group of values for θ_1 was chosen, making θ_2 and θ_3 equal to zero. The simulated and measured *TARCs* of the array are presented in Figures 10(c) and 10(d).

Also, in Figure 11, the simulated *TARC* reaches a system bandwidth from 2.92 to 4.65 GHz, while the measured one shows a system bandwidth from 3.32 to 4.19 GHz for values less than -10 dB, demonstrating that the proposed array performs adequately for MIMO applications without degrading the stipulated bandwidth when different signals arrive at the antenna.

Figure 12 presents the normalized measured and simulated gain patterns, where the peak measured gain approximates -2 dBi, also showing a quasi-omnidirectional pattern on the H-plane and nulls close to 0° and 180° on the E-plane. The size reduction of an antenna has the imperative drawback of either decreasing the bandwidth or/and the gain. It has been explained in different papers that a negative gain (in dB) is expected for size-reduced antennas [15–18].

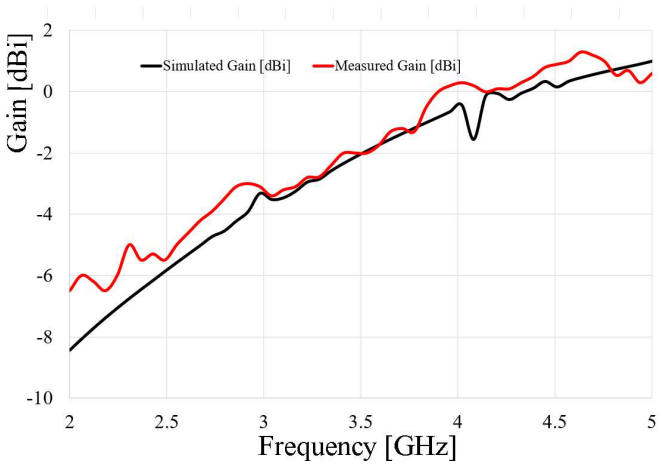

FIGURE 13. Comparison of simulated and measured gain of the MIMO antenna.

Figure 13 presents the comparison of the simulated and measured gains over the operational bandwidth, in which a convergence of results and behavior of this parameter is observed.

Finally, Table 1 shows a comparison of different 4-element MIMO antennas and the work proposed here.

In Table 1, to make a fair size comparison, all proposals are related to their corresponding wavelengths in free space, according to their operation frequencies. In this table, it is observed that the published antennas present similar characteristics regarding MIMO metrics compared to this work; however, it must be pointed out that [2] and [10] show an incomplete result of the *TARC*, since in those graphics the proper analysis is not made by selecting different random phases, as described in (8), displaying just one curve. On the other hand, it is clear to note that the present work obtains great results even when the size is much smaller, and the individual elements of the array are much closer to each other (around 0.0613λ), showing an EM isolation among elements of around 25 dB at 3.5 GHz.

5. CONCLUSIONS

In the present work, a metamaterial-based 4-element MIMO antenna is presented, where the metamaterial effect is exploited to reduce the dimensions of the radiator, obtaining a size reduction of more than 75% compared to a conventional disc monopole operating at the same frequency. Besides, despite the closeness of the elements, the electromagnetic isolation reaches values above 25 dB for all the antennas, and the E-filed correlation, given by the *ECC*, is very small. On the other hand, the *TARC* presents values below -10 dB for bandwidth around 900 MHz, with a diversity gain close to 10. The antenna electromagnetic isolation is improved by a simple geometry of strip lines on the ground plane, behaving like electromagnetic walls, which are very easy to design and implement. Therefore, the main disadvantage of this configuration is the reduction of the gain, getting a measured value of -2 dBi, which is a trade-off that must be considered when size reduction, input matching, and bandwidth are the main goals.

REFERENCES

[1] Liu, X., J. Zhang, H. Xi, X. Yang, L. Sun, and L. Gan, "A compact four-band high-isolation quad-port MIMO antenna for 5G and WLAN applications," *AEU-International Journal of Electronics and Communications*, Vol. 153, 154 294–154 303, Aug. 2022.

[2] Moses, A. T. Z., N. Moses, and D. K. Janapala, "An electrically small 4-port self-decoupled MIMO antenna pairs operating in n78 5G NR band for smartphone applications," *AEU-International Journal of Electronics and Communications*, Vol. 145, 154 082–154 090, 2022.

[3] Sufian, M. A., N. Hussain, H. Askari, S. G. Park, K. S. Shin, and N. Kim, "Isolation enhancement of a metasurface-based mimo antenna using slots and shorting pins," *IEEE Access*, Vol. 9, 73 533–73 543, May 2021.

[4] Ghosh, S., G. S. Baghel, and M. V. Swati, "Design of a highly-isolated, high-gain, compact 4-port MIMO antenna loaded with CSRR and DGS for millimeter wave 5G communications," *AEU-International Journal of Electronics and Communications*, Vol. 169, 154 721–154 729, Sep. 2023.

[5] Li, Y., L.-A. Bian, K.-D. Xu, Y. Liu, Y. Wang, R. Chen, and S. Xie, "Mutual coupling reduction for monopole MIMO antenna using L-shaped stubs, defective ground and chip resistors," *AEU-International Journal of Electronics and Communications*, Vol. 160, 154 524–154 534, Feb. 2023.

[6] Sharma, M., N. Mishra, and R. K. Chaudhary, "SRR based compact wideband metamaterial inspired antenna for WiMAX (2.5–2.7)/WLAN (2.4–2.48)/Bluetooth (2.4–2.48)/LTE (2.3–2.4) applications," *Progress In Electromagnetics Research Letters*, Vol. 80, 109–116, 2018.

[7] Mishra, N. and R. K. Chaudhary, "A compact CPW fed CRR loaded four element metamaterial array antenna for wireless application," *Progress In Electromagnetics Research*, Vol. 159, 15–26, 2017.

[8] Mishra, N., A. Gupta, and R. K. Chaudhary, "A compact CPW-fed wideband metamaterial antenna using Ω-shaped interdigital capacitor for mobile applications," *Microwave and Optical Technology Letters*, Vol. 57, No. 11, 2558–2562, 2015.

[9] Su, L., J. Naqui, J. Mata-Contreras, and F. Martín, "Modeling and applications of metamaterial transmission lines loaded with pairs of coupled complementary split-ring resonators (CSRRs)," *IEEE Antennas and Wireless Propagation Letters*, Vol. 15, 154–157, 2015.

[10] Vélez, A., J. Bonache, and F. Martín, "Varactor-loaded complementary split ring resonators (VLCSRR) and their application to tunable metamaterial transmission lines," *IEEE Microwave and Wireless Components Letters*, Vol. 18, No. 1, 28–30, Jan. 2008.

[11] Gatea, K. M., "Compact ultra wideband circular patch microstrip antenna," in *2012 First National Conference for Engineering Sciences (FNCES 2012)*, 1–5, Baghdad, Iraq, Nov. 2012.

[12] Chen, X., T. M. Grzegorczyk, B.-I. Wu, J. Pacheco, and J. A. Kong, "Robust method to retrieve the constitutive effective parameters of metamaterials," *Physical Review E*, Vol. 70, 016608, Jul. 2004.

[13] Fritz-Andrade, E., A. Pérez-Miguel, J. A. Tirado-Méndez, L. A. Vásquez-Toledo, R. Marcelín-Jiménez, E. Rodríguez-Colina, and M. Pascoe-Chalke, "Discrete formulation of envelope correlation coefficient for faster analysis in MIMO antenna systems," *Ingeniería, Investigación Y Tecnología*, Vol. 23, No. 4, 1–14, 2022.

[14] Fritz-Andrade, E., H. Jardon-Aguilar, and J. A. Tirado-Mendez, "The correct application of total active reflection coefficient to

evaluate MIMO antenna systems and its generalization to N ports," *International Journal of RF and Microwave Computer-Aided Engineering*, Vol. 30, No. 4, e22113, Apr. 2020.

[15] Wheeler, H. A., "Fundamental limitations of small antennas," *Proceedings of the IRE*, Vol. 35, No. 12, 1479–1484, Dec. 1947.

[16] Bokhari, S. A., J. F. Zurcher, J. R. Mosig, and F. E. Gardiol, "A small microstrip patch antenna with a convenient tuning option," *IEEE Transactions on Antennas and Propagation*, Vol. 44, No. 11, 1521–1528, Nov. 1996.

[17] Staub, O., J.-F. Zürcher, and A. K. Skrivervik, "Low profile, confortable, printed slot antenna for mobile communications," in *Proceedings of the Journées Internationales de Nice sur les Antennes, JINA'98*, 104–107, Nice, Nov. 1998.

[18] Zürcher, J. F., O. Staub, and A. K. Skrivervik, "Antenne Bi-Fréquence pour Pieced'Horlogerie," Swiss Patent submission No. 2000 0488/00 and European Patent submission No. 00200934.8.

[19] El-Din, M. S. H. S., S. I. Shams, A. M. M. A. Allam, A. Gaafar, H. M. Elhennawy, and M. F. A. Sree, "SIGW based MIMO antenna for satellite down-link applications," *IEEE Access*, Vol. 10, 35 965–35 976, 2022.

[20] Sufian, M. A., N. Hussain, A. Abbas, J. Lee, S. G. Park, and N. Kim, "Mutual coupling reduction of a circularly polarized MIMO antenna using parasitic elements and DGS for V2X communications," *IEEE Access*, Vol. 10, 56 388–56 400, 2022.

[21] Chattha, H. T., "4-port 2-element MIMO antenna for 5G portable applications," *IEEE Access*, Vol. 7, 96 516–96 520, 2019.